Recoil Model contribution to W width Analysis

1st Year Transfer Report

Sarah Malik

University College London

June 21, 2005

Abstract

On production, the W bosons recoil against initial state gluons radiated by the quarks involved in the production of the boson. This initial state radiation and all the underlying events involved in the interaction represent the recoil model. It contributes as one of the biggest systematic uncertainties on the W width. This analysis focuses on determining a parameterisation of the recoil model using minimum bias and $Z \rightarrow e^+e^-$ events. A similar parameterisation with a few alterations will then be applied to the $W \rightarrow e\nu$ to reduce the uncertainty on the recoil model resolution and hence the W width

Contents

List of Figures

1. Motivation

The W width essentially gives the number of ways the W boson can decay and its branching fractions to those decays. The W width is extremely well predicted in the Standard model but it is also the least well checked part of the model. The Standard model predicts it to be: $\Gamma_W = 2.09 \pm 0.01 GeV$ The measurements of W width by various experiments are shown in the Figure 1.1.

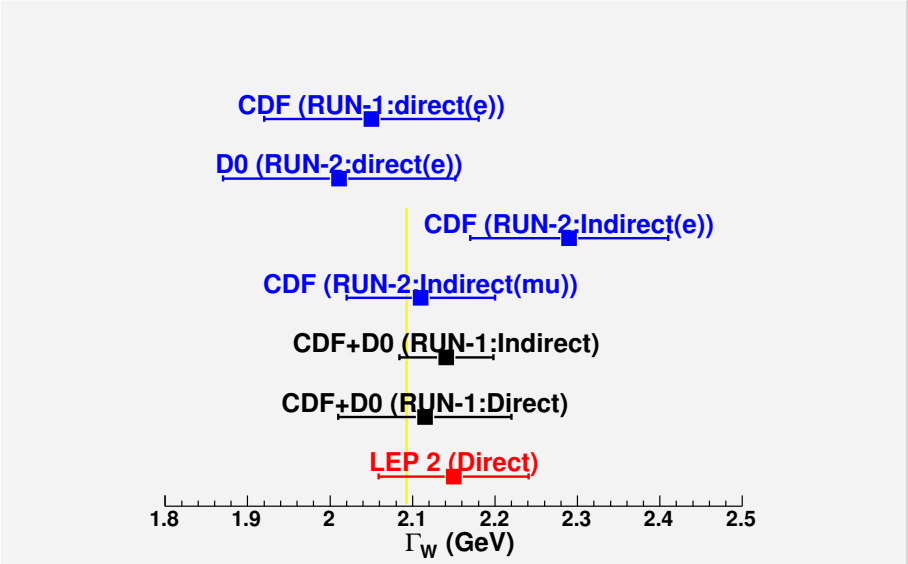

Figure 1.1: The direct and indirect measurements of W width as measured by CDF, D0 and LEP.

A discrepancy in the W width between the Standard model prediction and the measured value will point to some exotic decay modes of the W. Of course an additional advantage of a precision measurement of a quantity such as the W width means that we have unparallelled knowledge of our detector and how it works since it requires being painstakingly accurate in measuring energy scales and resolutions of calorimeters, calibration of tracking system and an in-depth understanding of the recoil [7].

2. Apparatus

This chapter is dedicated to the apparatus used to produce the W bosons and identify with precision the properties of the particles produced in its subsequent decay.

2.1 The Tevatron

The tevatron is the world's highest energy particle accelerator. It accelerates protons and anti-protons and collides them head-on in the two detectors, CDF and D0 at a centre-of-mass energy of 1.96 TeV. The primary sources of information for this chapter were the references [5],[6].

The acceleration and the final collision of the protons and anti-protons can be divided into several stages; proton acceleration, anti-proton production and acceleration and finally the collision at the 2 interaction points. These stages are shown in Figure 2.1 and briefly described below;

- H^- ions, which are essentially just hydrogen atoms albeit with an extra electron, are accelerated by the **Cockroft Walton** accelerator to 750keV.
- These are then injected into the **linac**, a linear accelerator about 130m in length, which accelerates them to 400MeV.
- The H^- ions are subsequently fed into the **Booster** where they are stripped of their electrons by passing them through a carbon foil. The resultant protons are accelerated to 8 GeV.
- The 8 GeV protons are fed to the **Main Injector**, a multipurpose synchrotron which accelerates them to a maximum energy of 150 GeV
- The final stage of the proton involves passing them through to the **Tevatron** where they are accelerated further, to a final 980 GeV and made to collide with anti-protons in the 2 detectors

Anti-protons, not being readily available, must be produced, stored until sufficient amounts are accumulated, then accelerated and fed into the Main Injector to share the fate of the protons.

- They are made by firing the protons from the Main Injector at a nickel target and selected from the shower of particles produced by using a bending magnet. They are then cooled, formed into a beam of anti-protons with a uniform 8 GeV energy and stored in the Accumulator until there is a sufficient quantity. They are then sent to the Main Injector where they

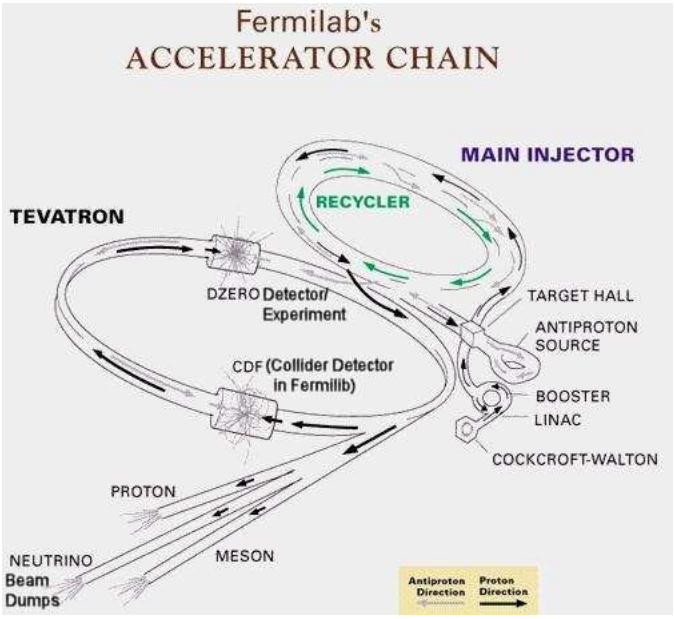

Figure 2.1: The Tevatron

circulate in an anticlockwise direction to the protons and accelerated to 150 GeV. They are subsequently passed to the Tevatron where they are accelerated further and made to collide with protons.

The final acceleration and collision of the protons and anti-protons occurs in the Tevatron, a 1km radius synchrotron ring using superconducting magnets, where the bunches are accelerated in opposite directions to 980 GeV and brought to collision at 2 points, the location of the CDF detector and the location of the D0 detector. The centre of mass energy of the collision is $\sqrt{s} = 1.96$TeV and the time in-between bunch crossings is 396 ns.

2.2 CDF Detector

The CDF Detector is a general multipurpose detector designed to study a broad range of interactions and final states produced in the p$\bar{p}$ collisions. An isometric view of the detector is shown in the Figure 2.2. The different sub-detectors that partake in the measurement of the particle energy, momenta and identification will be briefly discussed below with special emphasis on the components most relevant to this analysis.

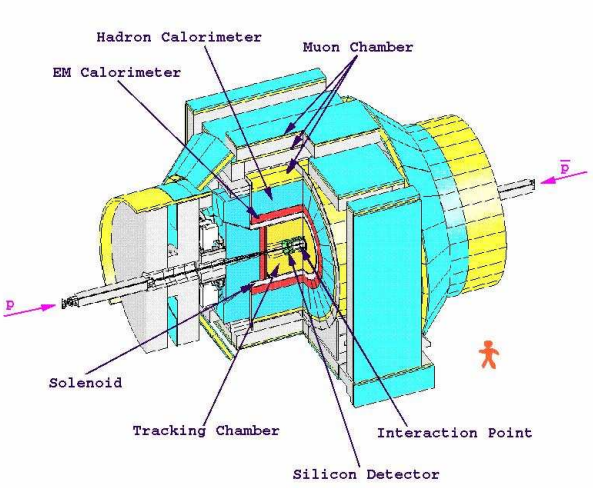

Figure 2.2: The CDF detector

2.2.1 Tracking System

The CDF detector consists of a Central Outer Tracker (COT), a 3m long drift chamber placed inside a 1.4 T magnetic field generated by a superconducting solenoidal magnet, that measures charged particle trajectories. It is filled with a mixture of argon, ethane and a small amount of alcohol such that charged particles traversing the material of the chamber produce ions and drift electrons. An electric field directs the drift electrons toward anodes on sense wires which give a precise position measurement. The sense wires are arranged on 8 superlayers. A silicon vertex detector placed very close to the beam collision point measures the position of charged particles very close to the interaction region with very high resolution. It is therefore useful in extrapolating a charged particle track to the collision point. This is very useful in heavy flavour decays which are characterised by secondary, displaced vertices very close to the primary interaction vertex.

2.2.2 Calorimeters

After the tracking comes the calorimetry system. This is divided in central, end and forward calorimeters which give a nearly 4π solid angle coverage. The Central Electromagnetic Calorimeter surrounds the COT and covers the pseudorapidity region $|\eta| < 1.1$. It contains alternating layers of scintillator and lead and is segmented into 24 wedges in ϕ for each half of the detector, 12 on the EAST and 12 on the WEST, with each wedge containing 10 electromagnetic towers. Each tower subtends 15^0 in ϕ and 0.1 in η. The calorimeter is crucial to the measurement of several of the decay modes used in the W width analysis, $W \rightarrow$

νe^{+-}, $Z \rightarrow e^+e^-$, similarly with the muon decay modes.There are also Plug Electromagnetic Calorimeter(PEM) which cover the region $|\eta| > 1$ and measure the energy deposited by particles travelling in the forward direction i.e at very small angles to the beam direction. The resolution in the CEM for electrons and photons is

$$\sigma_E/E = \sqrt{(0.135)^2/E_T + \kappa} \tag{2.1}$$

where the first term is called the stochastic term and the second term is called the constant kappa term [1]. The resolution in the PEM has a similar shape but these two terms have different values. Outside the CEM is the Central Hadronic calorimeter, CHA which measures the amount of energy deposited by hadronic jets as well as outgoing muons which tend to leave a small fraction of their energy in the CHA.

This system of calorimeters are crucial in calculating the transverse energy imbalance observed in the W decay modes in which a neutrino is produced. However, the system has several "cracks" or regions of low calorimeter response. These tend to occur at the boundaries of the different calorimeters, e.g between and central and plug calorimeters

2.2.3 Muon Chambers

The muon tracking chambers CMU surround the CHA and reconstruct the path trajected by the muons by the hits in the chamber.Since muons do not leave a significant energy deposit in the calorimeters and they are are minimum ionising particles(MIP) they travel through the detector relatively unscathed, with only hits in the muon chambers to confirm their presence.

The CDF coordinate system is defined with the z axis along the proton direction in the beam, the azimuthal angle ϕ is measured in the xy plane from x and the polar angle θ is measured in the yz plane from z. However, the variable η is more often used in place of θ. It is defined as $\eta = -log(tan(\theta/2)$.

3. W Width analysis

A direct measurement of the W width can be made from the shape of the transverse mass $M_T(e,\nu)$ distribution using the $W \to e\nu$ decay mode. It is worthwhile spending a moment here to define the transverse mass and the transverse energy, a quantity used later in the analysis. Although mass and energy are scalar quantities, the transverse mass used is analogous to the invariant mass except only the components transverse to the beam line are used. Similarly, the transverse energy is simply the transverse component of the vector with the energy of the particle defined as the magnitude of the vector and the momentum being parallel to the direction of the vector [1]. Transverse quantities are used because they can be measured more accurately, whereas longitudinal components of momenta which escape at very small angles to the beam line are not detected. Neither is the neutrino, whose presence must be inferred from an energy imbalance in the transverse plane.

The transverse mass of the W can be defined as;

$$\left(M^W{}_T\right)^2 = \left(E^l{}_T + E^\nu{}_T\right)^2 + \left(p^l{}_T + p^\nu{}_T\right)^2 \tag{3.1}$$

where $M_T{}^W$ is the transverse mass of the W, $E_T{}^l$, $E_T{}^\nu$ are the transverse energies of the electron and neutrino respectively and, $p_T{}^l$, $p_T{}^\nu$ are the transverse momentum vectors of the lepton and neutrino [1]

In order to achieve a good precision on the width it is therefore necessary that all the quantities that alter the transverse mass distribution are well understood. These quantities and their contribution to the systematic uncertainty on the W width for run 1 data and the projected uncertainties for run2 are shown in the table below [8].

In the $W \to e\nu$ decay mode, the electron is detected by its track in the COT and the energy it deposits in the CEM while the presence of the ν is inferred by the transverse energy imbalance in the calorimeter. An accurate determination of the energy scale in the calorimeter and the momentum scale in the tracking system is therefore crucial to the W width measurement.

The production of the W boson with a transverse momentum, p_T must be balanced by the transverse momentum of recoiling hadrons produced in association with it. This hadronic recoil is measured in the calorimeters and is used, together with the electron energy deposit in the calorimeter to calculate the transverse energy of the neutrino. It must therefore be modelled accurately and the detector response to the recoil energy calibrated.

	run 1		run2	
Source	**e**	**mu**	**e**	**mu**
Recoil + W pT	80	115	40	60
Lepton Scale/Non-linearity	65	15	35	10
Backgrounds	30	50	20	30
Detector Model/Lepton-ID	30	40	20	25
Lepton Resolution	10	20	5	5
PDF's	15	15	10	10
QED	10	10	10	10
Mw(40MeV)	10	10	10	10
total	115	135	65	75
Combined	90MeV		50MeV	

Selection criteria are applied to reduce background contamination from events that can mimic the $W \to e\nu$ signature, e.g $W \to \tau\nu$, $Z \to e^+e^-$ and multijet background events. The residual backgrounds or the remaining contaminations are estimated and used to determine the systematic uncertainty on the width [2].

The measured transverse mass $M_T(W)$ spectrum is then fitted to Monte Carlo, generated at a range of Γ_W. All the above effects that change the $M_T(W)$ distribution are required to be included in the simulation.

This analysis will be concentrating mainly on the recoil model and determining a parameterisation of it for $Z \to e^+e^-$ events which can then be attuned to develop a similar model for the W events.

3.1 Central Tracker momentum scale and resolution

Muons are used to calibrate the COT from a sample of $Z \to \mu^+\mu^-$ events. The muon decay mode is preferred for this calibration as it has a smaller contribution from bremsstrahlung than the electrons. The reconstructed Z mass obtained from the 2 high p_T tracks of the muons is normalised to the world average Z mass, which is known to a precision of 2.1 MeV [1][4]. The momentum scale obtained using the Z sample is extrapolated to obtain the scale for the W's, we therefore require the response of the COT to the muon momentum to be linear. Checks on the reconstructed Z mass and momentum scale are performed by using several low mass resonances and their decays to muons e.g J/ψ and upsilon, as these are copiously produced at the Tevatron [1].

3.2 Calorimeter energy scale and resolution

The electron energy scale is set by using the $Z \rightarrow e^+e^-$ decay mode. It can be calibrated as before by normalising the reconstructed mass of the e^+e^- pair to the world average value of the Z mass. The width of the Z mass distribution is used to measure the electron resolution in the calorimeter [1]. Corrections are made for the non-uniformity of the calorimeter response. This non-uniformity is dependent on various parameters, for instance energy loss in the material of the solenoid, shower leakage which in turn depends on the shower energy and on the position of the centre of shower with respect to the centre of the wedge. These corrections can be made by a comparison of the electron track momentum and the energy it finally deposits in the CEM. A plot of E/p, ratio of the energy deposited by the electron in the CEM and its curvature/momentum in the COT, against time and the azimuthal angle ϕ exhibits the non-uniformity. E/p is a very useful quantity. It can be used to calibrate both the CTC and CEM [2]. It is used in the alignment of the CTC using the CEM by analysing the difference in the E/p distribution for positive and negative leptons [2]. Since the CEM is unbiased to charge, the energy deposited by opposite charged particles in the CEM should be equal, whereas their curvature and hence the momentum in the COT may be different. Similarly, the fact that the COT response is relatively linear can be exploited to calibrate the CEM, where the response varies from tower to tower [2]. We require the energy response of a calorimeter to stay constant with time, i.e the energy it displays in response to a particular energy deposit at a specific time should be equal to the energy reported by it in response to that same energy deposit at a later time.

3.3 The Recoil Model

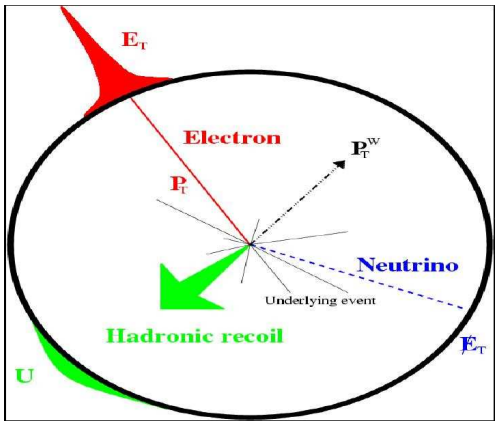

Figure 3.1: A schematic diagram of the W boson decaying into an electron and a neutrino and recoiling against gluon[3].

The recoil energy receives contributions from two fundamental sources; initial state QCD radiation, i.e gluons radiated from the incoming partons that produce the vector bosons and underlying event energy.

Hard QCD sub-processes A hard QCD sub-process is a process in which a high transverse momentum p_T vector boson, a gluon, is exchanged between an incoming parton from the p and the $\bar{p}$ [9]. A feynman diagram of the process is shown in Figure 3.2. The initial state QCD radiation mentioned above is therefore the gluon and it is this that the W boson recoils against so the p_T of the gluon is equal in magnitude and opposite in direction to the p_T of the boson. It is therefore strongly dependant on boson p_T.

soft underlying event This includes all the underlying low p_T interactions, for instance, multiple interactions, spectator parton interactions and remnants of the $p\bar{p}$ collision [9].

bremsstrahlung photons Bremsstrahlung photons radiated from charged leptons can contribute to recoil if they are not emitted collinear with the lepton and thus end up in a different calorimeter tower from the lepton. A feynman diagram for the process is shown in Figure 3.3.

A recoil energy vector **u** is defined as the sum of the transverse energy vectors of all the particles recoiling against the W in the p$\bar{p}$ collision. It is calculated by summing over the transverse energies of all the towers in the calorimeters (equation 3.2 [2]). The lepton towers are subtracted from the sum, so for W

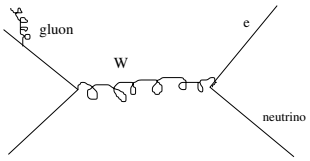

Figure 3.2: Feynman diagram showing the W boson recoiling against a gluon radiated from an incoming quark.

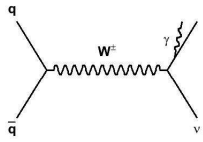

Figure 3.3: Feynman diagram showing brehmsstrahlung from the electron produced in $W \to e\nu$ decays [3]

events, energy of one electron is excluded, in Z events two electrons are excluded from the total.

$$\mathbf{u} = (u_{p_x}, u_{p_y}) = \Sigma_i E_i sin\theta_i (cos\phi_i, sin\phi_i) \tag{3.2}$$

Since there are two major contributions to $\mathbf{u}$ it is convenient to divide it into two components, u_1 which is parallel to the p_T of the W boson and u_2 which is perpendicular to it. The parameterisations of these two components are discussed in more detail in the next chapter.

3.4 Backgrounds

A number of events can contribute to the background in a $W \to e\nu$ sample by faking the signal. We discuss these and the rejection criteria applied to reduce this background and obtain pure sample.

- $Z \to e^+e^-$

  The $Z \to e^+e^-$ can fake the $W \to \nu e$ event and contaminate the sample if one of the two electrons falls into a region of low calorimeter response, e.g a crack, thus the energy deposit reported will be very small. So this electron will very often be mistaken for the neutrino and the lack of a substantial energy deposit in the calorimter will fake missing energy. This background can be reduced with help from the CTC which gives good coverage and efficient tracking efficiency in regions where most of the cracks are found [2]. The CTC is used to search for a track, whose momentum together

with the first electron will give a reconstructed invariant mass close to M_Z. Evensts such as these are then removed from the sample. The number of residual $Z \to e^+e^-$ background events remaining in the W sample can be estimated by allowing a number of Monte Carlo $Z \to e^+e^-$ events to pass through the W selection criteira and then counting the number that go through without being identified [2].

- **QCD Background**

  A QCD background event contains hadronic jets, a dijet event can contaminate the sample if one of the jets mimics an electron and the other is poorly measured so that it resembles a missing energy. This type of background can be reduced by using the track isolation variable which gives the number of tracks within a cone specified by η and ϕ around the electron track and cutting on this variable. It is required to be zero for a clean sample of W electrons [2].

- $W \to \tau\nu \to e\nu\nu\nu$ The process $W \to \tau\nu \to e\nu\nu\nu$ resembles a $W \to \nu e$ event but with substantially reduced electron E_T, and transverse mass and at a rate that is substantially lowered by the branching fraction of $\tau \to e\nu\nu\nu$ such that few of these events end up in the W sample, however they are the largest contributors to the background. There is also a small background from events in which the τ decays hadronically [2].

4. Results and Conclusions

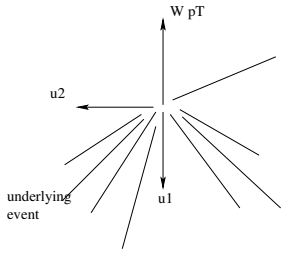

Figure 4.1: A diagram showing the parallel(u1) and perpendicular(u2) components of the recoil

As mentioned in the previous chapter, a convenient way of modeling the response and resolution of the recoil model is to divide the recoil energy into parallel and perpendicular components, as shown in Figure 4.1. u_1 receives a contribution from the initial state gluon radiated by the quarks. This is what the W boson recoils against and it is therefore expected to be strongly dependant on p_T with a small contribution from underlying events. It can be parameterised as

$$u_1 = f(p_T) + G(UE) \tag{4.1}$$

, where f is some function of the vector boson p_T and G is a function of the resolution on underlying event energy. The resolution on u_1 is also therefore dependant on p_T of the boson.

The component perpendicular to the vector boson p_T, u_2 is principally dominated by underlying events. This manifests itself in ΣE_T, the sum of the transverse energy deposited in all the calorimeter towers in an event. Since information on the instantaneous luminosity is not generally available for every event, ΣE_T is used to characterize the response and resolution of underlying events. Figure 5.1 shows the mean ΣE_T plotted in ranges of luminosity. It can be seen that the mean transverse energy deposited in the calorimters increases as the luminoisty increases. An increase in instantaneous luminosity results in a greater number of intereactions taking place per beam crossing, hence more energy is deposited in the calorimteres. The component u_2 is therefore expected to be, on the whole, independent of p_T with a zero mean,and a resolution dependant only on luminosity . Fits to the u_1 and u_2 distributions in bins of p_T in Figure5.3 show that resolutions for both can be approximated by gaussian. It can be parametrised as:

$$u_2 = H(UE) \tag{4.2}$$

where H is a function of the resolution on underlying event energy

The u_2 resolution can be understood by the distribution shown in Figure 5.2 which is essentially a plot of the σ of the underlying energy in x direction, i.e σ_x against luminosity. The resolution decreases with increasing luminosity. This is to be expected since an increased luminosity gives a greater ΣE_T for the event.

Equation 2.1 from section 2.2.2 gives the parameterization of the calorimeter resolution as a function of E_T. It is defined here again.

$$\sigma_{E_T}/E_T = \sqrt{(0.135^2)/E_T + \kappa} \tag{4.3}$$

This relationship shows that σ is approximately proportional to $\sqrt{E_T}$.

The distribution of $\sigma_{x,y}$ against ΣE_T for minimum bias data seems to be well described by a simple power law, which looks very similar to the above relation. The distribution is shown in figure 5.4 and is fitted with the relation;

$$\sigma(u) = 0.3998(\Sigma E_T)^{0.5079} \tag{4.4}$$

Figure 5.4 therefore gives us the calorimeter response to minimum bias events, which as mentioned in the previous chapter is one of the dominant contributions to the recoil model.

The QCD contribution to the recoil can be analysed by first taking a look at the $Z \rightarrow e^+e^-$ events. The Z data gives u_1, u_2, ΣE_T and the Z p_T, which is reconstructed from the p_T of the 2 electrons and is thus the smeared p_T not the true Z p_T. In W events, only the p_T of the electron and the energy of the recoil is measured. The parameters used to construct the recoil model above can therefore be derived by fitting to the variables obtained from the Z data [1]. The 2 components of the recoil energy vector can be plotted as a function of the boson p_T. Figure 5.5 shows the mean and sigma of the u_1 component in bins of Z p_T, with a linear fit to both distributions. The mean of u_1 increases linearly with p_T. This is because transverse momentum conservation requires the gluon recoil to balance the p_T of the boson. The underlying event contribution was expected to be minimal and from the plot it seems to appear as a constant in the parameterization of u_1. The sigma of u_1 is shown to increase with the Z p_T since the hadronic recoil energy deposited in the calorimeters is greater and thus from equation 2.1, σ is greater.

Figure 5.6 shows the mean and sigma of the u_2 component in bins of Z p_T. The mean of the distribution is almost zero, so this component has little dependence on boson p_T. The sigma distribution is somewhat unexpected. However, this dependence on p_T can be explained by higher order QCD effects. It is possible that at high p_T, the Z boson recoils against more than one gluon, traveling in different directions. The direction perpendicular to the resultant Z p_T will therefore include contributions from hadronic recoil.

The brehmsstrhalung contribution to the recoil model, not mentioned so far, has been looked at briefly in Figures 5.7 and 5.8, which shows the transverse mass distribution for the muon and electron channel for W events in the simulation. The blue curve is the M_T with no final state photon radiated and the red curve is the M_T with one final state photon. Any shift in the transverse mass is not obvious since the energy of these photons is low. The next step will be to evaluate the contribution of this effect to the recoil by fitting templates of different Γ_W to this and quantifying any shift in transverse mass.

5. Evaluation and Future plans

The next step in the analysis will be to use the parameters derived by fitting to the Z data to construct a model of the recoil in the simulation. The simulation then needs to be run on the parameterisation , the χ^2 for all the parameters minimised and then this minimised χ^2 parameterisation compared to data. As mentioned above, the p_T of the Z measured in the event is the smeared p_T not the true p_T. This must be accounted for, by somehow undoing the smearing effect, caused by measurement error on the electrons in the calorimeters, to get the true p_T. It may also be instructive to fit to the variables provided in the muon channel and compare the parameterisation obtained to the electron channel.

The u_1 sigma and mean distributions in bins of p_T have so far only been fitted with a first order polynomial and although the two distribtuions give good χ^2 it will be good to fit them with a quadratic to get a more sound understanding of the Z p_T dependance. Similarly, the u_2 sigma distribution can be fitted with a non-linear fit.

Ultimately, we want to use the parameterisation of the recoil model obtained using the Z events and apply it to the W's. We are assuming that because the W and Z bosons are quite close together in mass, their true p_T distributions will be similar with only the difference in the masses to account for. However, their measured p_T distributions are different since the Z bosons are measured from 2 elecrons and the W is measured from the electron and the recoil. So in the W data, the recoil is defined with respect to the direction of the electron p_T, the parallel component of u is the component along the direction of the electron p_T and the second component is that perpendicular to the lepton p_T. So when the final paramterisation of the model is applied to W events, all these factors will have to be taken into account.

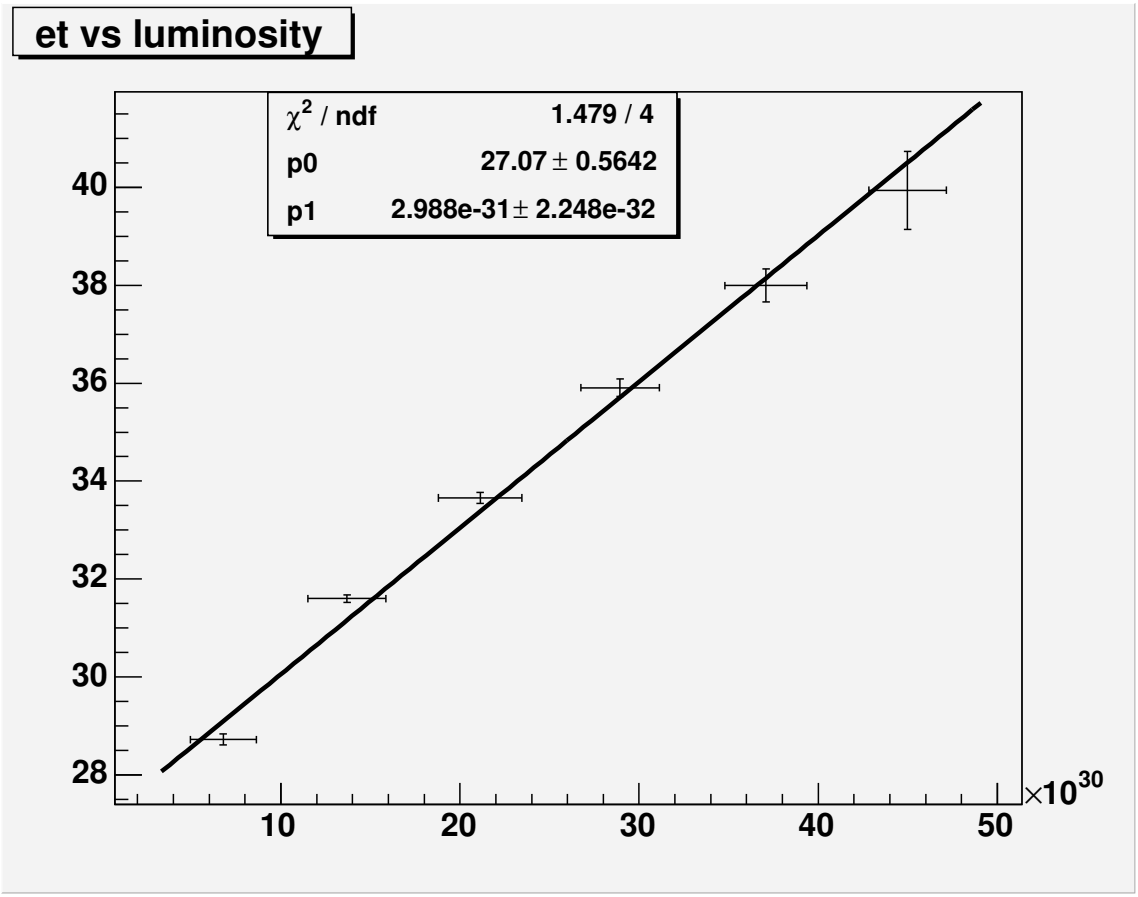

Figure 5.1: The mean ΣE_T in bins of luminosity

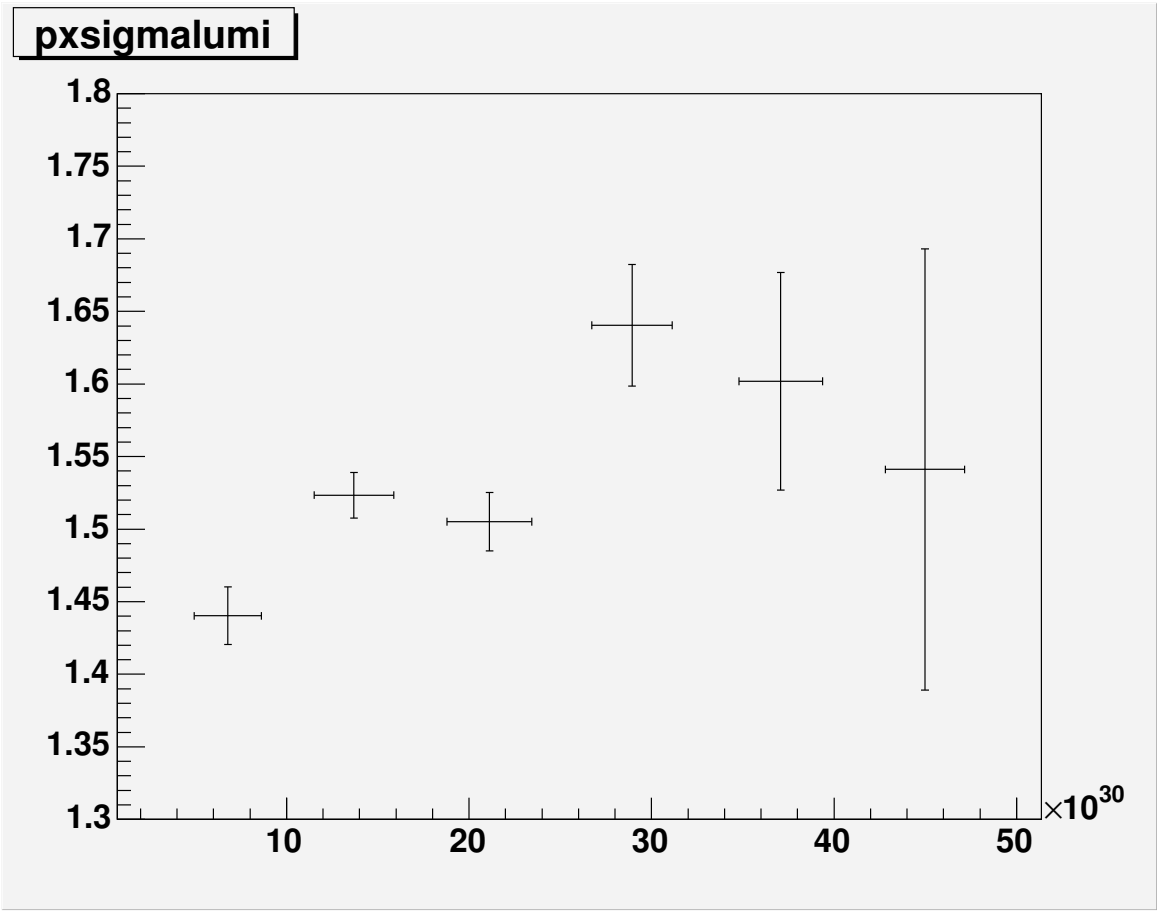

Figure 5.2: The sigma of energy deposited in x in bins of luminosity

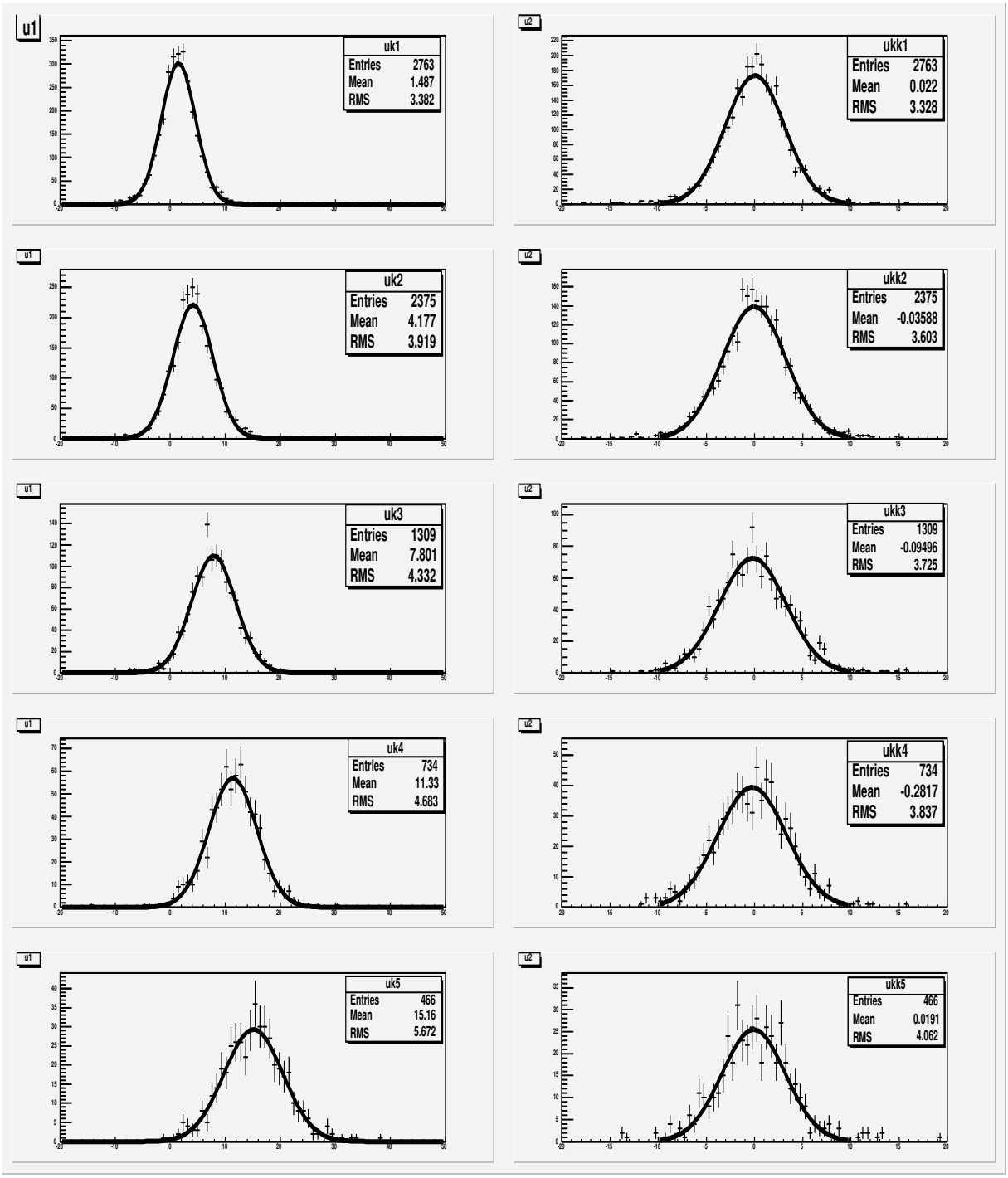

Figure 5.3: The u_1(left) and u_2(right) distributions plotted in bins of Z p_T, with ranges, 0 - 5GeV, 5-10GeV, 10-15GeV, 15-20GeV and 20-25GeV, from top to bottom

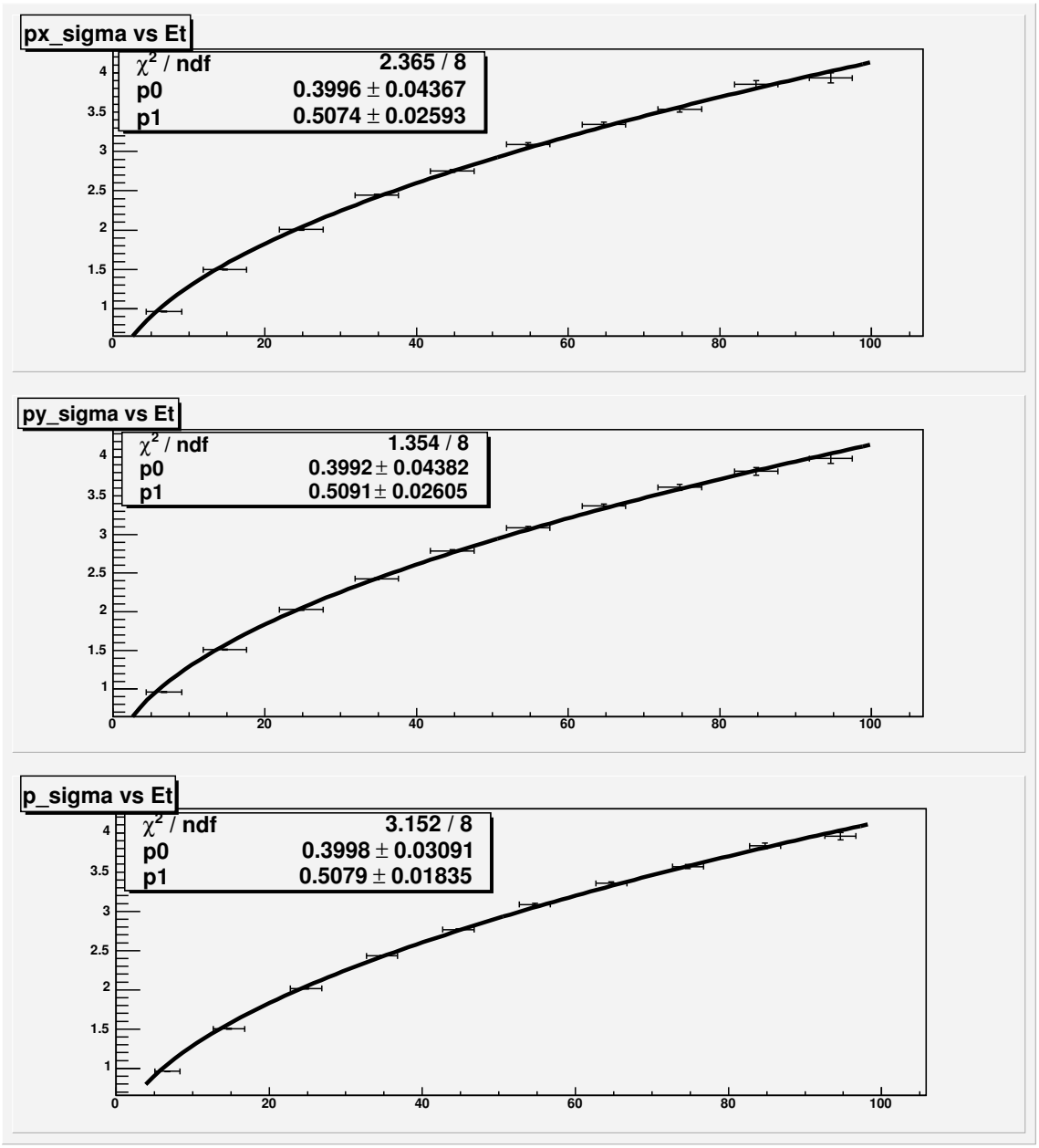

Figure 5.4: $\sigma_{x,y}$ in bins of ΣE_T distributions (top and middle) and the average σ in the x and y directions against ΣE_T for minimum bias events

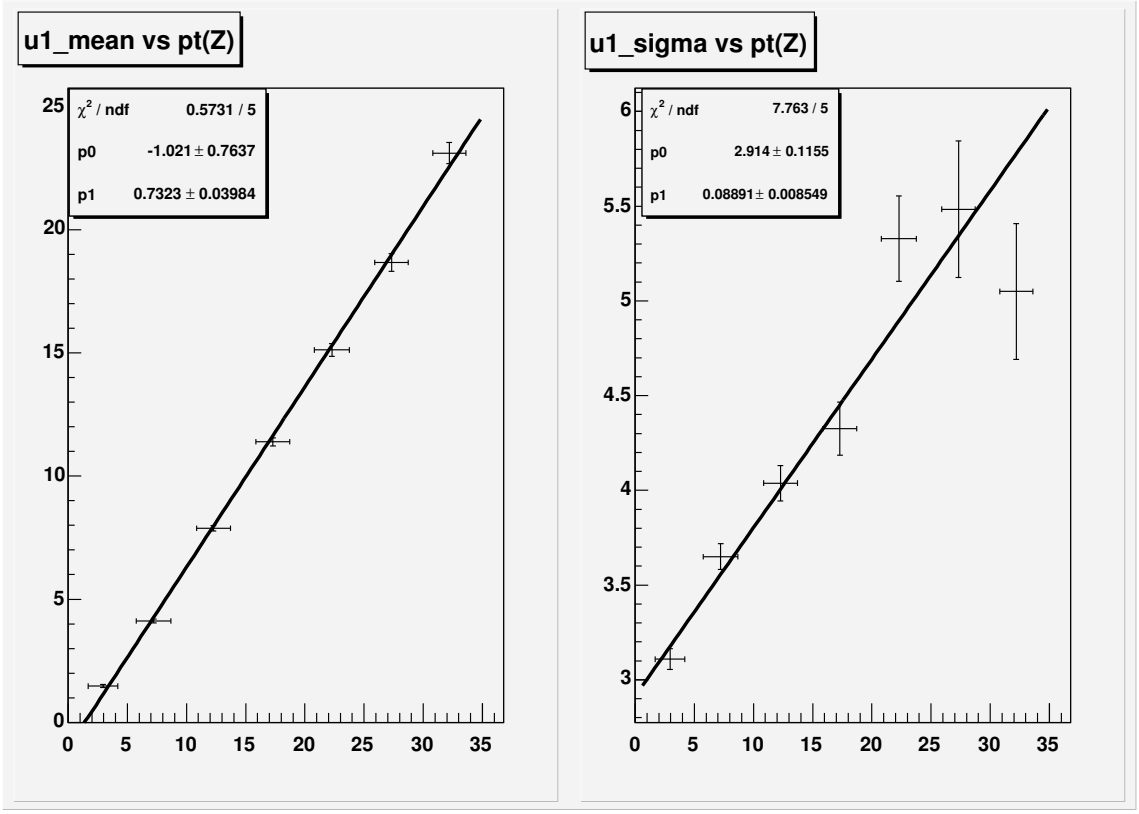

Figure 5.5: The mean and σ of u_1 in bins of p_T of Z

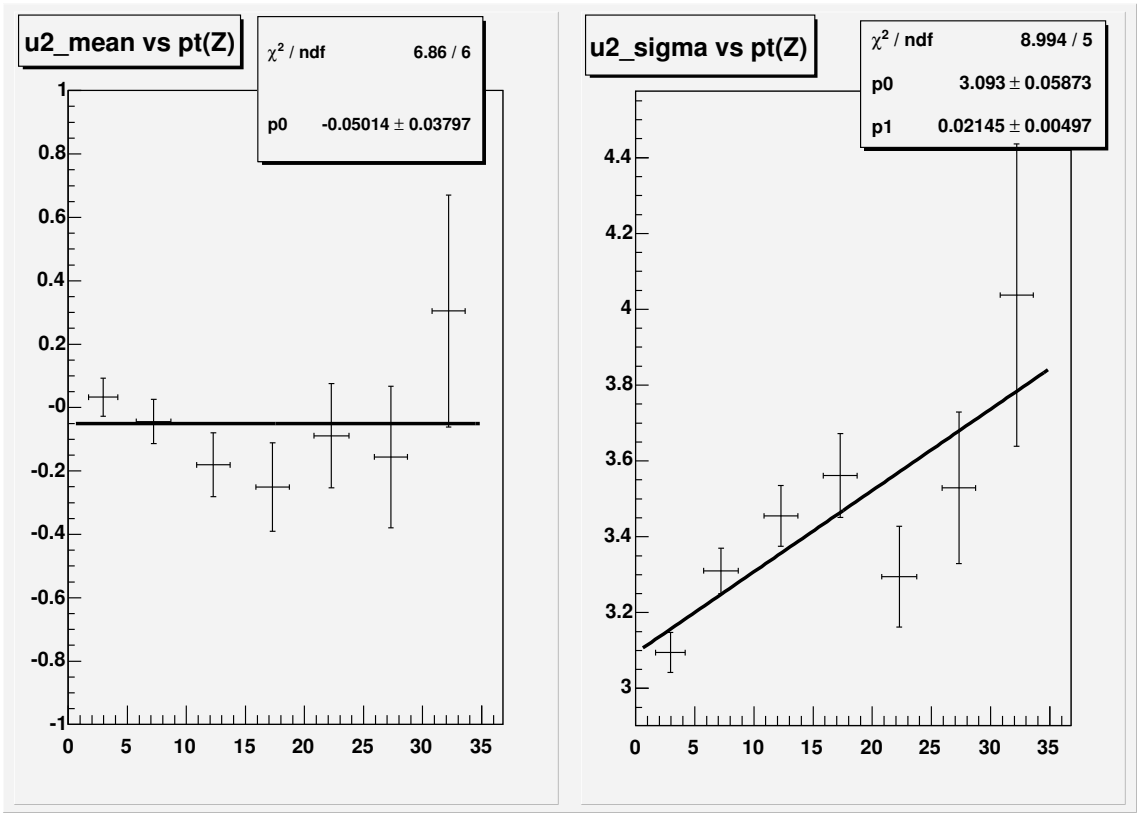

Figure 5.6: The mean and σ distributions of u_2 in bins of p_T of Z

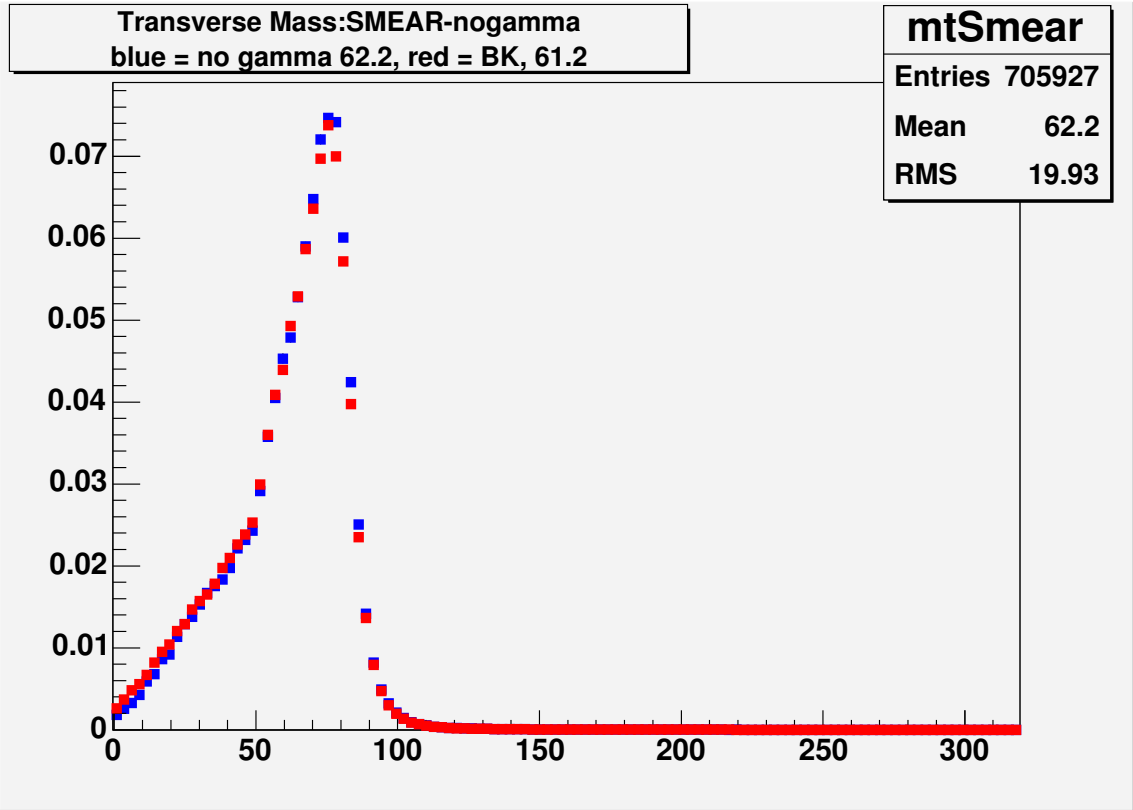

Figure 5.7: Transverse mass distribution in the electron channel for no final state photon(red) and with one radiated photon(blue) in the simulation

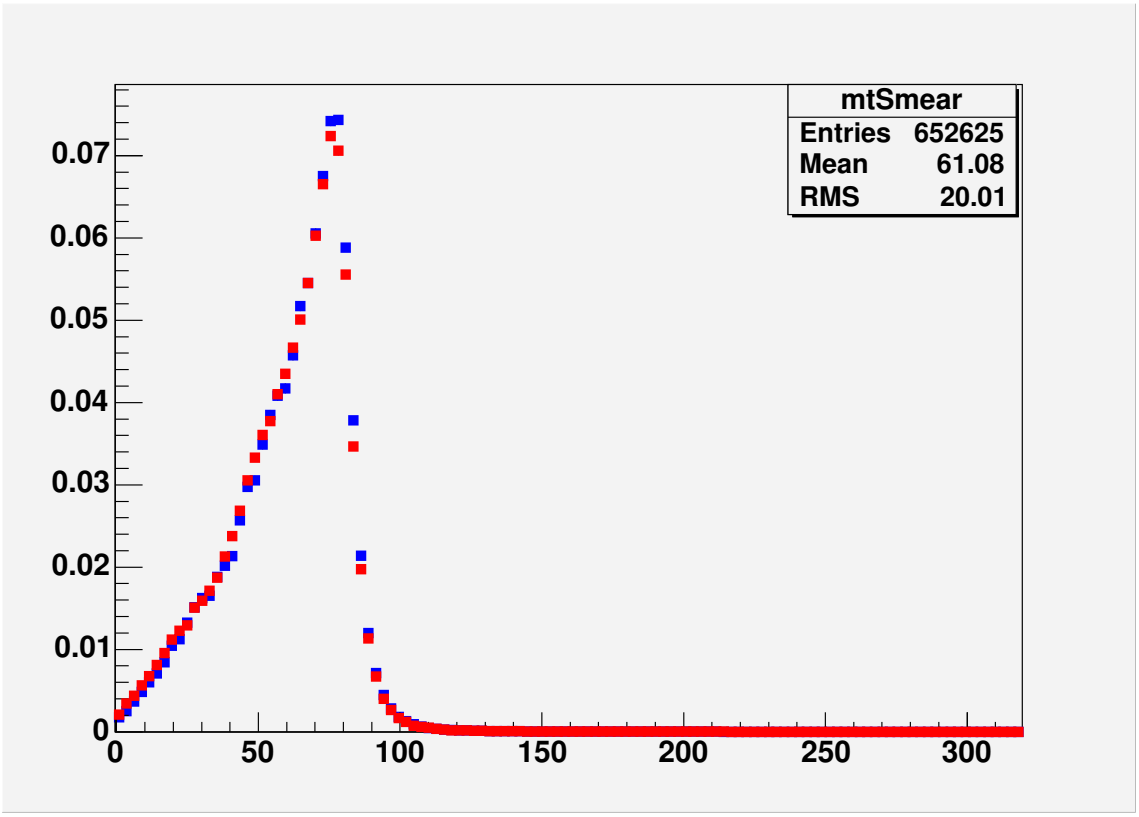

Figure 5.8: Transverse mass distribution in the muon channel for no final state QED radiation(red) and with one photon radiated(blue) in the simulation

Bibliography

[1] Measurement of the W Boson Mass with the Collider Detector at Fermilab, CDF/ANAL/ELECTROWEAK/CDFR/5184 (2000)

[2] William Joseph Ashmanksas, A Direct Measurement of the W Boson Decay Width in Proton-Antiproton Collisions at 1.8 TeV (1998)

[3] Chris Hays, W Boson Mass Measurement at the Teavtron, CDF and D0 collaborations (2005)

[4] Particle Data Group (2004)

[5] Erik Matthews Brubaker, A Measurement of the Mass of the Top quark in Lepton + Jet Events at CDF, CDF/THESIS/TOP/PUBLIC/7624 (2004)

[6] Aidan Robson, A Measurement of Z Boson Production and Rapidity Distribution in proton anti-proton collisions at $\sqrt{s} = 1.96$ TeV, CDF/THESIS/ELECTROWEAK/PUBLIC/7509 (2004)

[7] Larry Nodulman, Talk on W Mass, CDF Collaboration Meeting, Barcelona, May 2005

[8] Mark Lancaster, A Direct Measurement of W width, 2004

[9] Troy Vine, First Year report , 2004